Hindawi
Advances in Civil Engineering
Volume 2023, Article ID 7508814, 14 pages
https://doi.org/10.1155/2023/7508814

Research Article

Improved Shape-Finding Method and Parametric Study for Designing Asymmetric Suspension Bridges in Mountainous Terrain

Chenchen Jiang,[1] Yangxun Ou,[1] Weiyu Tang,[1] Shengjun Hou,[1] Rui Luo,[2] Yuhao Jin,[2] and Bin Sun [2]

[1]*China Power Construct Road and Bridge Group Co. Ltd., Beijing, China*
[2]*Department of Bridge Engineering, Tongji University, 1239 Siping Road, Shanghai 200092, China*

Correspondence should be addressed to Bin Sun; sunbin@tongji.edu.cn

Received 17 February 2023; Revised 4 July 2023; Accepted 31 July 2023; Published 14 August 2023

Academic Editor: Giosuè Boscato

The suspension bridges in mountainous areas are commonly designed with asymmetrical overall layouts to match the terrain and construction under limited space. However, the effects and influences of the asymmetry parameters on the bridge performance have yet to be thoroughly investigated. To address this gap, based on a real-world suspension bridge with a main span length of 700 m, this paper first presents an improved shape-finding method that can fully consider the components of hanger forces in each construction step. In the iterative process, the shape of the cable is determined based on the equilibrium equations, and the hanger forces are calculated through the nonlinear finite element analysis. After deciding the bridge's initial state, the asymmetry parameters' effects are carefully investigated through finite element analysis under the static and seismic conditions. Results show that the side-to-span ratio of the main cable and the tower's stiffness can affect the horizontally constrained stiffness, resulting in distinct bridge behavior. Moreover, reasonably designing the dampers between the tower and the girder can be beneficial in minimizing the longitudinal displacement and controlling the tower's moment under the seismic situations.

1. Introduction

Suspension bridges are preferred to satisfy the long navigation width requirement due to their advantages in spanning capacity, construction, and esthetics. Most completed suspension bridges cross seas, bays, or rivers, while long-span bridges spanning deep canyons are relatively rare. However, with the construction of high-grade highways and high-speed railways in western China, the number of large-span suspension bridges in mountainous areas is expected to proliferate. To match the undulating landforms, suspension bridges in mountainous areas are often designed with asymmetric layouts. The asymmetric characteristics include the height of towers, side span lengths, etc., The mechanical performance of asymmetric suspension bridges in mountainous areas can be significantly different from the traditional suspension bridges because the constrained stiffness of the main cable on the two sides is quite unequal [1]. The inherent nonlinearity of the suspension system adds to the complexity of analyzing and optimizing asymmetric suspension bridges in the mountainous regions. Therefore, a sufficient understanding of the mechanical performance of an asymmetric suspension bridge is essential for the practical design.

Some scholars have investigated the performance of suspension bridges through a parametric study. As main cables are the primary load-carrying components of the suspension bridges, the configuration of the main cable must be determined based on the force equilibrium between internal member forces and dead loads to reach the ideal finished bridge state before the parametric study, and this process is referred to as "shape finding" [2]. Some advanced shape-finding methods have been proposed in the recent years. For instance, Kim and Lee [3] proposed an analytical formulation that took the unstained cable length as an unknown parameter, thus eliminating the iterative process. Kim and

Kim [4] introduced the initial force method to consider the deformations of the girder and towers. Kim et al. [5] improved the above two methods for the initial shape analysis of 3-dimension cables. Xiao et al. [6] present a five-step algorithm extended from the common finite element method (FEM) analysis method with the additional algebraic operation and flow control to analyze the initial shape of spatial cables. Song et al. [7] extended Xiao's method to the spatial cable system. Li et al. [8] developed an analytical algorithm for the main cable system with high-convergence efficiency, where the self-weight of the cables can be directly considered. Li and Liu [9] simplified the unknown variables in shape finding into a concise shape with only three unknowns, which is easily solved by Interacting Influence Matrix (IIM) optimization. Zhou and Chen [10] proposed finding the target profile of cables by nonlinear analysis conducted on the bridge structure, and two iteration schedules were introduced. Zhu et al. [11] developed a novel shape-finding method for the main cable of a suspension bridge using a nonlinear finite element approach with an Eulerian description. As for self-anchored bridges, Wang et al. [12] proposed a shape-finding method for self-anchored suspension bridges considering the axial deformation of the girder. Sun et al. [13] proposed an initial shape analysis formula called the coordinate iteration method for a self-anchored suspension bridge whose main cable is three-dimensionally curved. Existing methods can complete the reasonable finished state analysis of the suspension bridges, and the results are acceptable in engineering [14]. However, most shape-finding methods consider the cable an independent member subject to several concentrated loads from the hanger. These methods do not deal with the construction steps of the bridge, and this causes an error between the calculated value and the actual value of the hanger force. The effect of the construction method on hanger forces is significant for the suspension bridges in mountain areas, as more complex steps will be employed due to poor transport conditions. To increase the accuracy of the initial shape of cables, the effect of the construction method on the internal forces of bridge members should be adequately considered.

On the other hand, based on the developed shape-finding method, some researchers have investigated the design parameters to optimize the structural performance. Wang et al. [15] compared the differences between carbon fiber reinforced polymer (CFRP) cables and steel cables on the static response of the suspension bridges. Jia et al. [16] and Lijun et al. [17] developed a finite element model to investigate the impacts of tower stiffness, sag-to-span ratio, side-midspan ratio, and tower-girder connection mode on the bridge's mechanical parameters. For a three-tower four-span double-deck steel truss suspension bridge, Cheng et al. [18] investigated the impact of various structural parameters on the static and dynamic behavior of the entire bridge and the mechanical performance of the deck system. Cao et al. [19] studied the deformation of a three-tower suspension bridge with a central buckle under live loads. The influence of the sag-to-span ratio of the cable, the girder's stiffness, and the cable's slippage were analyzed. For asymmetrical suspension bridges, Zhang et al. [1] proposed an analytical method to calculate the cable shape in the completed bridge state under live load action and free cable state for a triple-tower suspension bridge with two asymmetrical spans, and the construction parameters were considered. The seismic response of a 780 m single-span suspension bridge with viscous dampers was investigated by Zheng et al. [20]. The above studies provide a comprehensive analysis of the mechanical performance of suspension bridges. However, it is worth noting that only a few studies have been conducted on asymmetric suspension bridges. Therefore, the effect of the regularity of parameters with asymmetric characteristics on the structure's response under static and earthquake still needs to be explicit.

Regarding dynamic performance, wind, and seismic effects are critical to the safety of large span suspension bridges in mountainous areas. The impact of wind on the suspension bridges includes vibrations, torsion, wind loads, and aerodynamic effects [21, 22]. These influences can increase stress, damage the structure, and reduce stability [23]. Wind-resistant design measures and structural considerations need to be implemented to ensure the safety of suspension bridges [24, 25]. Moreover, seismic events can induce the ground motion that affects the dynamic response of suspension bridges, mainly when seismic waves propagate through the bridge piers and cables. Such vibrations can impose the significant additional stresses on the bridge structure, potentially leading to structural damage or collapse [26, 27]. The horizontal displacements and ground deformations caused by earthquakes can induce relative displacements between the bridge towers and the deck, further exacerbating the stress levels and compromising the overall structural integrity of the bridge. Therefore, it is crucial to implement the robust design measures and structural interventions to ensure the safety and resilience of suspension bridges against seismic hazards [28]. To limit the relative displacement between the tower and girder to absorb and dissipate the vibrational energy caused by wind or seismic events, dampers are commonly installed between the towers and girders of the suspension bridges. However, when the heights of the bridge towers are different, there can be a significant disparity in the support stiffness of the dampers on both sides, which may adversely affect the structure's internal forces and displacement response [29]. Therefore, the selection of damper parameters is crucial in asymmetric systems.

This paper concerns the shape-finding method and parameter study of long-span asymmetric suspension bridges in mountain areas to overcome the gaps. An improved shape-finding method that can accurately consider various construction steps is proposed in this paper. The efficiency and accuracy of this method are demonstrated using a 700 m single-span asymmetric suspension bridge as an example. Moreover, the influence of asymmetric design parameters on the structure's static performance and natural frequencies is investigated. The role and appropriate parameters of dampers between the tower and girder of asymmetric systems in typical seismic conditions are analyzed. Conclusion remarks are drawn at the end of this paper.

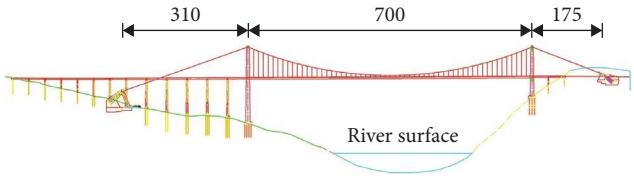

Figure 1: The general layout of the bridge (unit: m).

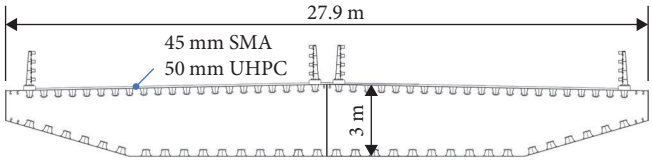

Figure 2: Cross-section of the stiffening girder.

Table 1: Cross-sectional properties.

Cross-section	A (m^2)	I_z (m^4)	I_y (m^4)	J (m^4)
Girder (per separate)	1.3417	99.0577	1.9311	5.4649
West tower (top)	39.2000	102.4427	160.0667	211.2748
West tower (bottom)	96.5275	673.9023	894.6342	1291.3860
East tower (top)	39.6480	103.6134	165.6176	215.6184
East tower (bottom)	52.2480	341.9202	379.0109	136.5414

*Note: A, cross-section area; I_z, moment of inertia to the z-axis; I_y, moment of inertia to the y-axis; J, torsion resistance.

2. Engineering Background

2.1. Bridge Overview. A practical suspension bridge in Yunnan Province of China is considered the engineering background for shaping the findings and further investigation. The span arrangement of the main cable is 310 + 700 + 175 m. The towers' west and east sides are 181 and 120 m high, respectively. Figure 1 depicts the bridge's overall configuration.

In the midspan, the planes of the two main cables are parallel. The main cable has a sag of 70 m and a center transverse spacing of 27 m. The theoretical splay point of the west anchorage is 310 m away from the central line of the west bridge tower. In contrast, the theoretical splay point of the east anchorage is 175 m away from the central line of the east bridge tower. Hangers have a typical longitudinal spacing of 12 m.

Figure 2 shows the detailed design of the stiffening girder. As noticed, the central height of the girder is 3 m with a width of 27.9 m. Table 1 illustrates the section properties of the stiffening girder and the top and bottom sections of the towers.

2.2. Finite Element Model. A finite element model of the example bridge is established in SAP2000. The main cable and hangers are simulated using cable elements, and the stiffening girder and towers are simulated using beam elements. The tower's bottom and the anchor points of the main cables are fixed; the transverse and vertical degrees of freedom are coupled between the tower and the girder, and all degrees of freedom are coupled between the tower's top and the main cable.

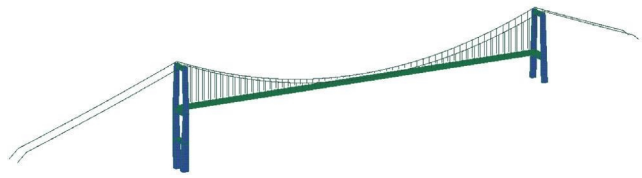

Figure 3: The finite element model of the whole bridge.

The model of the entire bridge has 1,132 nodes and 709 components. Figure 3 depicts the full bridge's finite element model.

3. Improved Shape-Finding Method

3.1. Framework. An improved shape-finding method is first presented in this section for determining the initial equilibrium state of the bridge before the parametric investigation. The internal force of each hanger in the finished form of a suspension bridge comprises two parts: the self-weight of the girder segments and a portion of the second stage dead load assigned according to the stiffness. The former can be estimated using the analytical equation, whereas the latter should be determined considering the construction process. Although the nonlinear FEM can be used to simulate the construction process, it is difficult for the FEM to consider local details such as the shape of saddles. Therefore, the main focus of the proposed improved shaping finding method is to establish an iterative procedure that combines the analytical equation and the finite element model for shape finding. Figure 4 depicts the main procedure of the proposed method. As noticed, the proposed method mainly consists of seven steps.

3.1.1. Determination of Hanger Force. To develop the finite element model, it is required to estimate the internal force of hangers first. Therefore, the first step of the analysis lies in preliminarily determining the initial force of each hanger.

First, by changing the hangers into continuous beam supports, as illustrated in Figure 5, a multispan continuous beam finite element model may be created to compute the preliminary internal force. The calculated preliminary internal force of the hanger is the support response derived by the finite element analysis.

Due to the small deviation between the preliminarily determined cable forces and the actual cable forces in the bridge's constructed state, as well as the minimal deviation in the cable shape and vertical stiffness, it is feasible to calculate the cable state, main cable shape, and unstressed length based on these cable forces in conjunction with the coordinates of control points. Subsequently, a finite element model is established to analyze the variations in cable forces caused by stiffness distribution during the construction under permanent loads in the second phase and the variations in cable forces resulting from anchor cable adjustments after bridge completion. Let the initial determination of cable force vectors be denoted as F_{H1};

Second, the final determination of cable forces in the bridge's constructed state is contingent upon two scenarios based on the actual construction method:

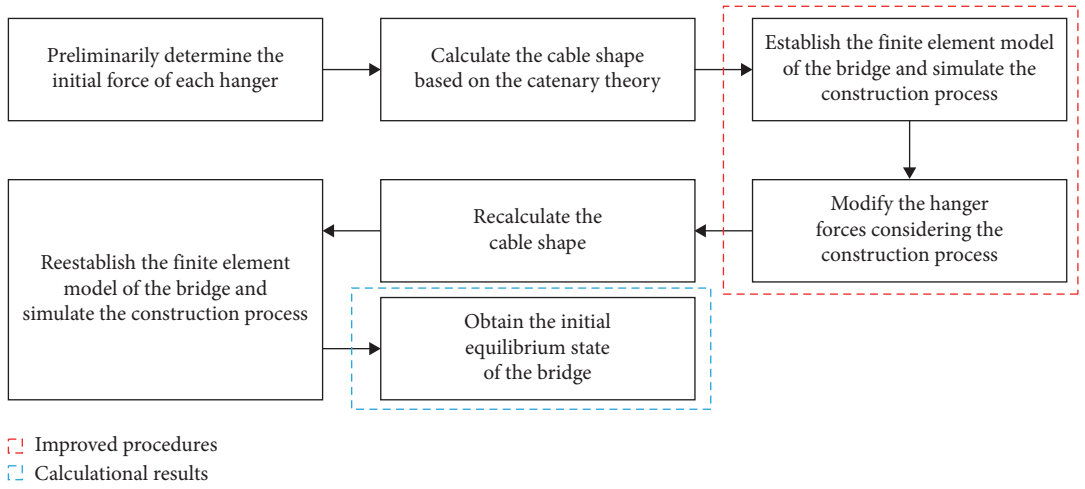

Figure 4: The determination process of the target finished bridge state.

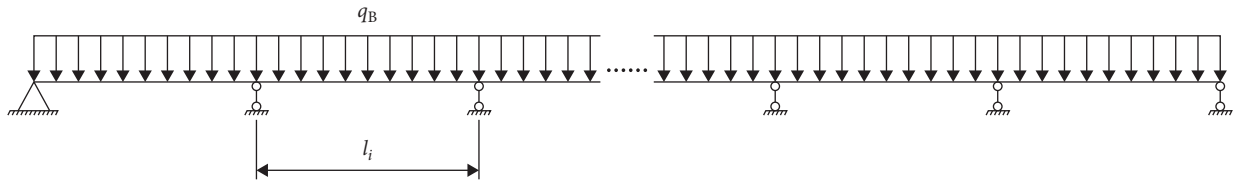

Figure 5: Calculation diagram of preliminary hanger force.

(1) If the cable forces cannot be adjusted after the second construction phase, the bridge deck paving, railing, and other permanent loads are applied in reverse to the main girder based on the bridge's constructed state model. Nonlinear finite element analysis is conducted to obtain the axial compression force F_{B2} in the main girder. If F_{B2} is not equal to 0, the modified value F_{H1} is used to recalculate the F_{B2} iteratively until it equals 0. This process yields the cable force vector F_{H2} corresponding to this state. The cable forces F_{H0} generated by the self-weight of the beam segments during articulation are determined by balancing the forces, resulting in the cable forces F_{H2} being determined as follows:

$$F_H = F_{H0} + F_{H1} - F_{H2}. \tag{1}$$

If the cable forces can be adjusted after the second phase of construction. In that case, the cable forces can be iteratively computed using the influence matrix method to minimize the bending moment energy in the main girder until the desired computational accuracy is achieved. The bending strain energy of the structure can be expressed as follows:

$$U = \frac{1}{2}\int \frac{M^2}{EI} ds. \tag{2}$$

In the finite element beam elements, it can be represented as follows:

$$U = \sum_{i=1}^{n} \frac{L_i}{4E_iI_i}(M_{Li}^2 + M_{Ri}^2), \tag{3}$$

where: n——the number of elements; L_i——the length of element i; E_i——the elastic module of element i; I_i——the moment of inertia of element i; M_{Li}——the bending moment at the starting end of element i; M_{Ri}——the bending moment at the ending end of element i.

Rewrite Equation (3) in matrix form as follows:

$$U = |M_L|^T[B]|M_L| + |M_R|^T[B]|M_R|, \tag{4}$$

$$B = \begin{matrix} \frac{L_1}{4E_1I_1} & \cdots & 0 \\ \vdots & \ddots & \vdots \\ 0 & \cdots & \frac{L_n}{4E_nI_n} \end{matrix}. \tag{5}$$

The left and right end moment vectors of the beam unit before cable force adjustment are denoted as $|M_{L0}|$ and $|M_{R0}|$, respectively. The influence matrices of cable forces on the left and right end moments of the beam unit are represented by $|C_L|$ and $|C_R|$. respectively. The adjusted left and right end moment vectors of the beam unit, denoted by $|M_L|$, can be expressed by the sum of the original vectors $|M_{L0}|$ and the vector representing the correction values of cable forces, denoted by $|\Delta T|$:

$$|M_L| = |M_{L0}| + |C_L||\Delta T|, \tag{6}$$

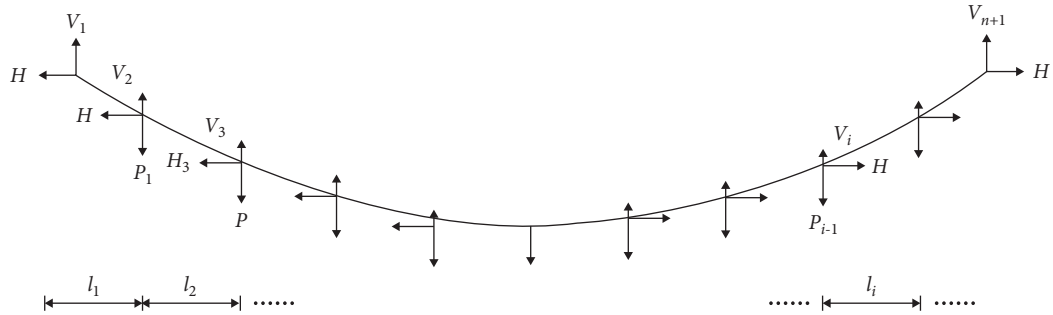

Figure 6: Calculation diagram of the main cable shape.

$$|M_R| = |M_{R0}| + |C_R||\Delta T|. \tag{7}$$

To minimize the bending strain energy of the structure after cable force adjustment, the following conditions must be satisfied:

$$\frac{\delta U}{\delta \Delta T} = 0. \tag{8}$$

By simultaneously solving Equations (4)–(8), the solution can be obtained as follows:

$$|\Delta T| = -\frac{|C_L|^T[B]|M_{L0}| + |C_R|^T[B]|M_{R0}|}{|C_L|^T[B]|C_L| + |C_R|^T[B]|C_R|}. \tag{9}$$

If the magnitude of vector $|\Delta T||$ satisfies the required computational accuracy, the iterative calculation process is completed. Otherwise, based on vector $|\Delta T|$, the cable forces at that moment are calculated, along with the corresponding cable sag profile. A nonlinear finite element analysis is then performed to obtain the left and right end moments of the beam unit at that moment. These calculated moments are the left and right end moment vectors of the beam unit before cable force adjustment. Subsequently, the aforementioned steps are repeated to recalculate the vector $|\Delta T|$. The cable forces corresponding to the $|\Delta T|$ that meets the computational accuracy requirements represent the final determined cable forces.

3.1.2. Calculation of Target Finished Bridge State. In the second step of the method, after obtaining the internal force of the hanger, combined with the material parameters and the coordinates of the design control points, the main cable shape of the suspension bridge in the completion state can be calculated. According to the suspension cable calculation theory, when the two ends of the suspension cable are fixed. The load is unshapely distributed along the cable length, the cable shape is a catenary. The functional relationship between the end coordinates of the cable segment, L and h, and the horizontal and vertical force, H and V at the end and the unstressed cable length S0 of the cable segment can be obtained as Equations (10) and (11):

$$l = \frac{HS_0}{EA} + \frac{H}{q_0}\left[\operatorname{arsh}\left(\frac{V}{H}\right) - \operatorname{arsh}\left(\frac{V - q_0 S_0}{H}\right)\right], \tag{10}$$

$$h = \frac{VS_0}{EA} - \frac{q_0 S_0^2}{2EA} + \frac{H}{q_0}\left[\sqrt{1 + \left(\frac{V}{H}\right)^2} - \sqrt{1 + \left(\frac{V - q_0 S_0}{H}\right)^2}\right], \tag{11}$$

where q_0 is the weight per unit length of the main cable, E is the modulus of elasticity of the main cable, and A is the main cable area.

When calculating the main span, start by assuming the shear force V and horizontal force H at the tangent point between the main cable and the left cable saddle, then separate it from the hanger and calculate the coordinate difference between the two ends and the unstressed length of each cable segment section by segment. Correct V and H based on the departure between the design value and the calculated value of the sag and the height difference between the left and right ends after the calculation to the right, and then recalculate using the same procedure until the deviation satisfies the accuracy standards. Figure 6 shows the calculation diagram for the main cable shape of the major span.

The horizontal force H can be considered a known quantity when the middle span computation is done. The main cable shape for the side span may then be computed similarly. The suspension bridge's primary cable shape has been calculated thus far.

However, note that the main cable shape and vertical stiffness can vary somewhat due to the difference between the preliminary internal force of the hanger estimated by this approach and the actual completion condition. Therefore, a finite element model is established in the third step of the method. Subsequently, in the fourth step, the change of the hanger force caused by the stiffness distribution during the second stage of deadly load application is determined based on the simulation of the construction process.

After modifying the hanger forces, considering the influence of the construction process, the fifth and sixth steps are similar to the second and third steps. The initial shape of the main cable in the completion state can be recalculated based on the calculation theory, and the finite element model is reestablished. Finally, in the last step, the above results can be provided for checking the bridge safety or as the initial

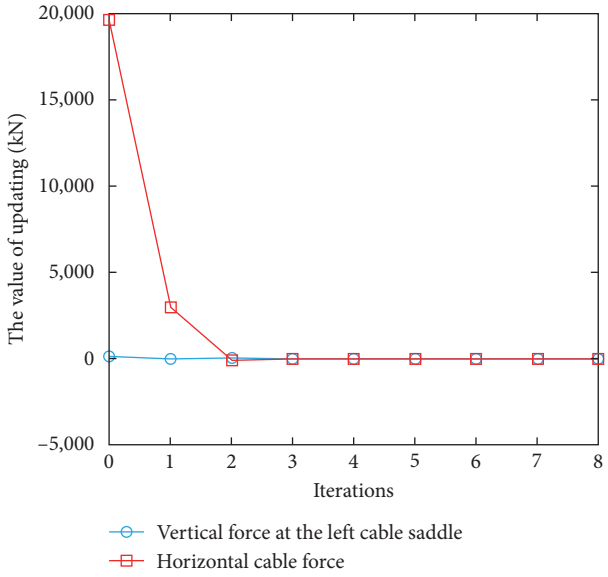

Figure 7: The convergence of updating parameters in the midspan.

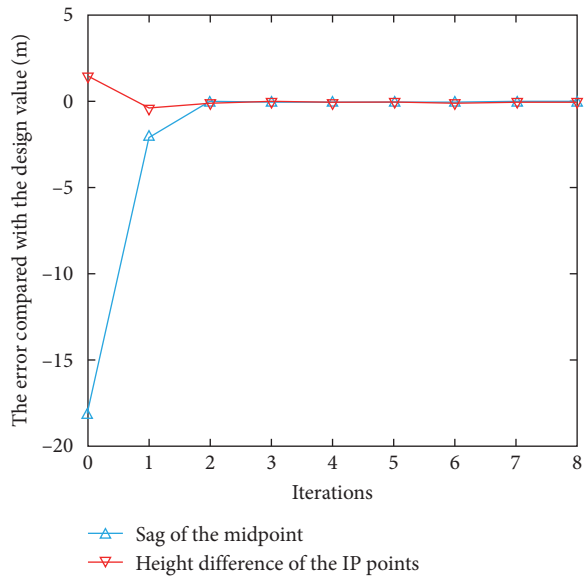

Figure 8: The convergence of control parameters in the midspan.

equilibrium state of the suspension bridge for further static or dynamic analyses.

3.2. Calculation Results. The unstressed length and line shape of each span's main cable are computed using the above-mentioned approach. Figures 7 and 8 depict the convergence processes of the updating and control parameters in the midspan, respectively.

The convergence speed for the iterative computation of the main cable shape is quite quick, as illustrated in Figures 7 and 8. The error for the achieved midspan sag is lowered to near zero after only one to two iterations, and the predefined stopping criterion (1 mm) can be reached with only eight iterations. Figure 9 depicts the moment of the stiffening of the girder in its completed shape.

The moment diagram of the stiffening girder after completion is remarkably similar to that of the continuous beam under dead load, as shown in Figure 9. The largest value of the bending moment arises at the point of the end hangers. The moments at all other positions are almost the same, demonstrating the precision of the determined completion state in this study. The above approaches are utilized in the follow-up research to determine the goal, finished bridge condition, and internal force of the suspension bridge for structural systems with various characteristics. The finite element model is built on this foundation for the future study.

4. Parametric Study

Based on the determined initial shape, the effects of some asymmetry parameters are investigated through the finite element (FE) model. Under static conditions, tower height and side span length influence bridge deformation and internal forces are analyzed. Subsequently, under seismic conditions, the effect of dampers is analyzed and suggestions for selecting proper damper parameters are given.

4.1. Horizontal Constrain Stiffness of Side Span System. The forces of the midspan main cable are always symmetrical due to its flexibility. The tension of the cable is transferred to the saddle and restrained by the side-span system, which is made up of the cable at the side span and the tower. The horizontal and vertical forces acting on the main cable in the midspan can be separated. In the vertical direction, the displacement is small due to the substantial axial stiffness of the tower, and it has a minor influence on the overall stiffness of the bridge. In the horizontal direction, the bridge tower and the main cables of the side span constitute a cantilever beam with the elastic support. The restraint stiffness is made up of the thrust stiffness of the tower and the geometric stiffness of the side-span main cables, which together resist the main cables' tension, as indicated in Figure 10. The asymmetry of the stiffness of the side-span restraint system leads to asymmetric displacements of the bridge under live loads. Considering that the tower's height and the angle of the main cable at the side span are unsymmetrical in the case study, the mechanical behavior of the bridge is studied based on these two factors.

4.1.1. Anchor Cable Angle. The ground-anchored suspension bridge described in this study has a single span and the anchor cable mostly carries axial stress and self-weight. The horizontal inclination of the connecting line between the tower top and the anchor point is referred to as the anchor cable angle. The main cables are fastened to the correct points on both banks according to the real topography in this segment, with varied anchor cable angles. The sinusoidal values of the anchor cable angle are 0.3, 0.35, 0.4, 0.45, and 0.5. Table 2 lists the parameter values. Figure 11 shows the parameter as well as the positions of anchor cables.

Figure 12 depicts the axial force of the main cable as a function of the anchor cable angle under dead load. The tension of the main cable in the center of the main span and at the top of the tower remains unchanged as the anchor

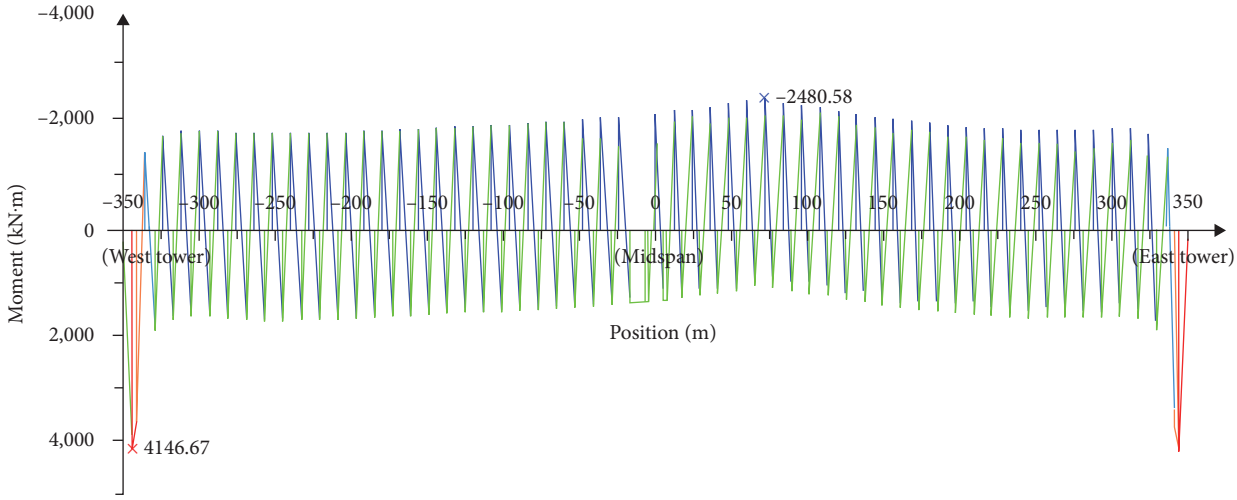

Figure 9: Distribution of bending moments along the stiffening girder (kN·m).

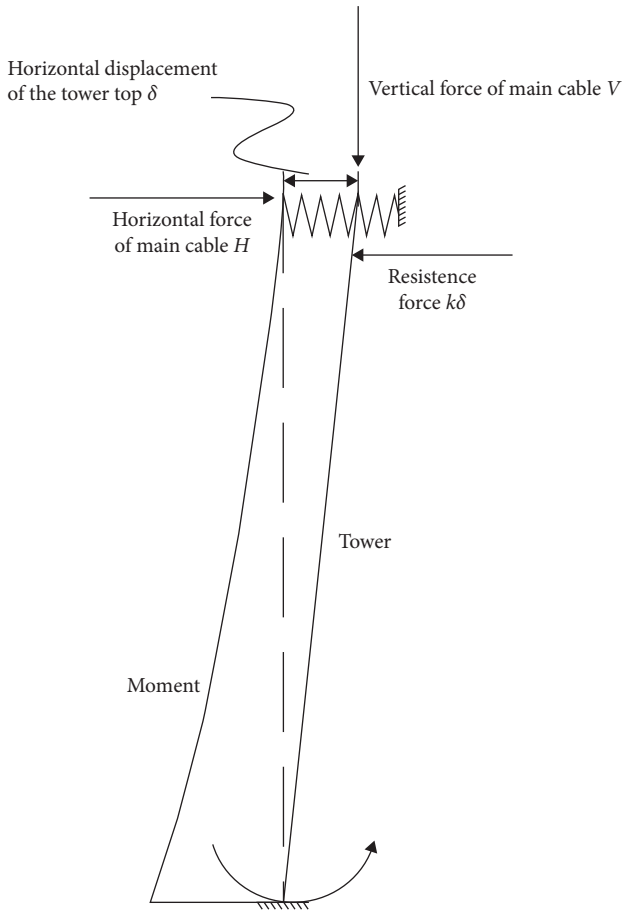

Figure 10: Illustration of the side-span constraint system.

cable angle rises; the tension of the anchor cable progressively increases.

The tension of the main cable in the main span is governed by the structure's self-weight distribution, as shown in Figure 12. The horizontal force of the main cable remains constant as the inclination angle of the anchor cable rises. However, the tension of the anchor cable is increased to offset the horizontal force of the main wire.

The deflection envelop of the girder in anchor cable angle under live load is shown in Figure 13. It can be observed that when the anchor cable angle increases, the stiffening girder's upward and downward deflections diminish. It demonstrates that raising the angle of the anchor cable increases the anchor cable's constraint on the bridge tower and stiffens the girder, which helps to improve the overall structural stiffness.

The trend of structural natural frequency variations due to changes in the side span-to-central span ratio is depicted in Figure 14. Alterations in the side-span ratio have discernible effects on the system's dynamic characteristics. Specifically, the corresponding frequencies exhibit an increasing trend for the positive/negative symmetric vertical bending modes and similar vibrational patterns as the side-span length extends, with changes of approximately 4% and 2%, respectively. Conversely, the frequencies associated with the positive/negative symmetric lateral bending modes remain largely unaffected by variations in the side-span length. Notably, the frequency of the first torsional mode experiences a decreasing trend as the side-span length increases, demonstrating a deviation of approximately 2%. Overall, the comprehensive analysis indicates that an increasing side-span length corresponds to a diminishing overall stiffness of the bridge, albeit gradually.

4.1.2. Tower Stiffness. The tower is a compression bending part that supports the main cable. The action on the tower is dominated by dead loads. The horizontal force of the main cable induced by dead loads can be balanced on the two sides after the bridge is finished. However, unbalanced tension forces can also be generated on the two sides due to the effect of live loads, resulting in a longitudinal displacement at the tower top. The rigidity of the tower has a considerable impact on the suspension bridge's live load equilibrium condition. The asymmetry of the tower stiffness

Table 2: Values of anchor cable angle parameters.

Number	The west bank		The east bank		The sinusoidal values of the anchor cable angle
	Height difference (m)	Distance between anchorage and tower (m)	Height difference (m)	Distance between anchorage and tower (m)	
(1)	101.52	338.41	62.84	209.48	0.3
(2)	108.86	311.03	65.75	187.84	0.35
(3)	115.10	287.75	68.10	170.26	0.4
(4)	120.47	267.71	70.06	155.69	0.45
(5)	125.14	250.28	71.71	143.41	0.5

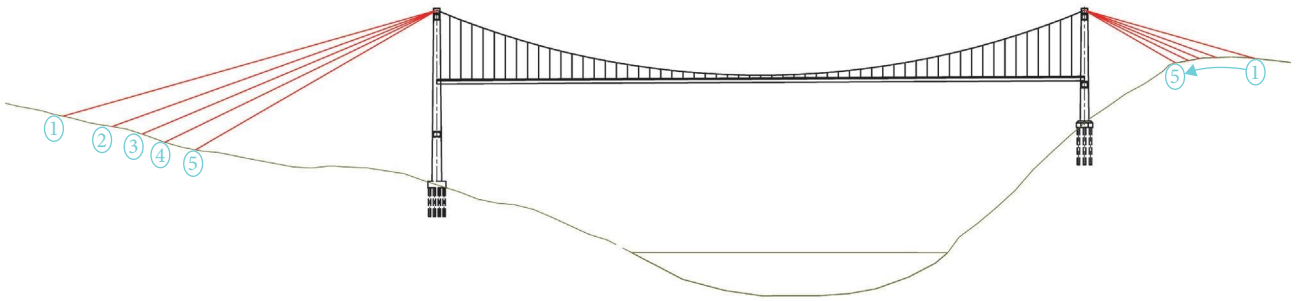

Figure 11: The position of anchor cables in varied angle.

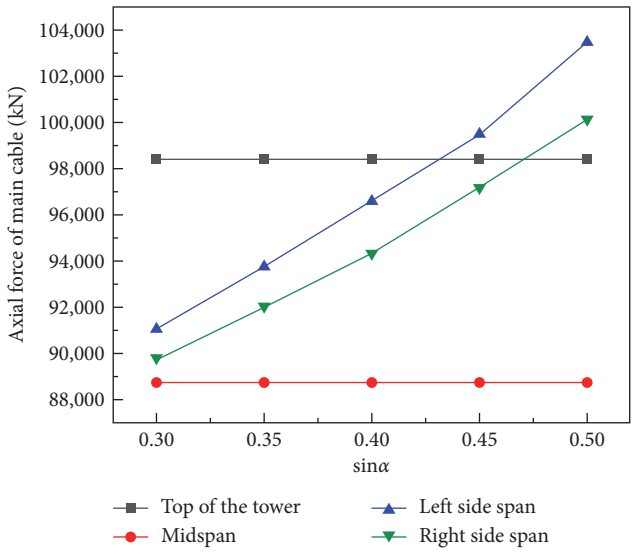

Figure 12: The change of the axial force of the main cable with the anchor cable angle under dead load.

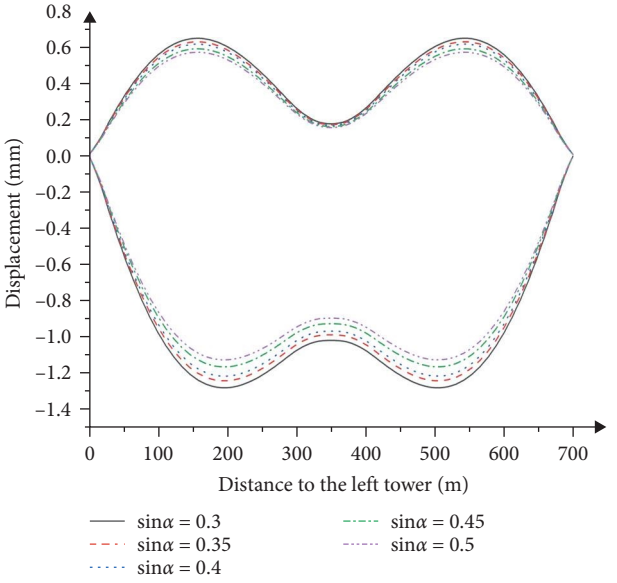

Figure 13: The change of stiffening girder deflection with anchor cable angle under live load.

may generate asymmetric structural deflections in a mountain suspension bridge.

To investigate this effect, the stiffness of the bridge tower is adjusted by keeping the wall thickness unchanged while maintaining the outer contour size of the section. Let δ denote the section size adjustment factor, that is, the multiple of the expansion or reduction of the section size. The values of δ are taken as 0.9, 1, 1.2, and 1.5, respectively, to study the influence of bridge tower stiffness on structural static and dynamic performance.

The influence of bridge tower stiffness on the bending moment under live loads is shown in Figure 15 (considering the left tower as an example). The moment of the bridge tower is about a straight line, as can be noticed. The moment of the bridge tower steadily increases as the rigidity of the tower rises. This demonstrates that the unbalanced horizontal force on the top of the bridge tower is the primary cause of the moment and that the increased stiffness of the bridge tower leads to the rise of the unbalanced horizontal force on the top.

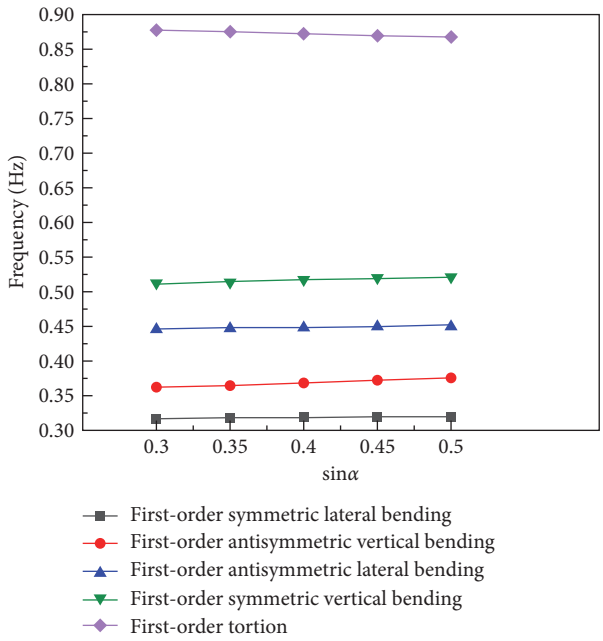

Figure 14: The change of natural frequency with anchor cable angle.

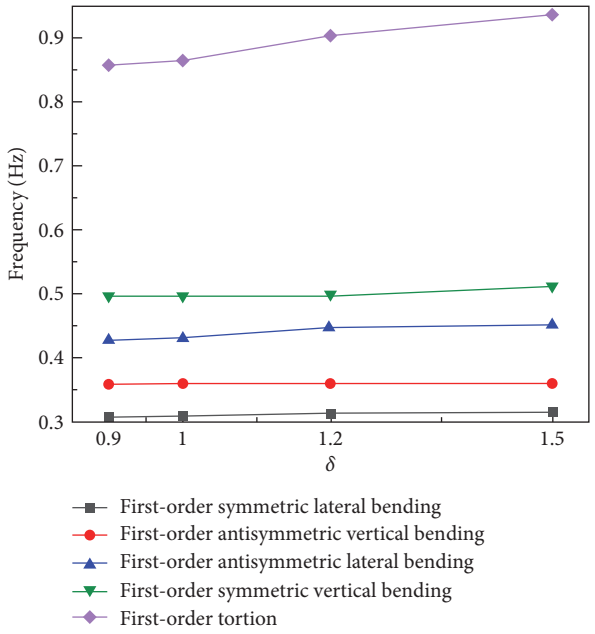

Figure 16: The change of natural frequency with tower's stiffness.

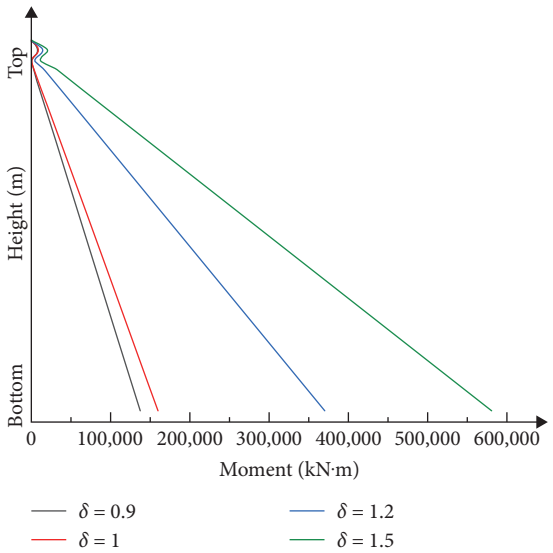

Figure 15: Influence of tower stiffness on tower moment (taking the west tower as an example).

The trend of structural natural frequency variations due to changes in the stiffness of bridge towers is depicted in Figure 16. The stiffness characteristics of the bridge towers primarily impact the torsional and lateral bending modes, with minimal influence on the vertical bending mode. Increasing the stiffness of the bridge towers leads to an augmentation in both the first antisymmetric lateral bending frequency and the first torsional frequency. Notably, the model with a section magnification of 1.5 displays an impressive 8.9% increase in the frequency of the first torsional mode. In comparison, the frequency of the first antisymmetric lateral bending mode experiences a substantial 5.6% increase compared to the model with a section magnification of 0.6. These findings demonstrate that enhancing the stiffness of the bridge towers can significantly improve the torsional and lateral bending stiffness of the bridge, thereby bolstering its resistance to the lateral wind loads. Furthermore, the increased torsional stiffness effectively mitigates the impact of coupled vehicle-bridge vibrations, further enhancing the overall performance of the bridge.

The impact of two "asymmetric" parameters on the fundamental mechanical behavior of the suspension bridge can be succinctly summarized as follows:

Firstly, the edge-span constraint system, composed of the bridge towers and the edge-span main cables, plays a critical role in constraining the horizontal displacement of the midspan main cables. Notably, the asymmetry of the bridge is primarily manifested through the asymmetrical horizontal constraint stiffness imposed by the edge-span constraint system on the midspan. An increase in the stiffness of the edge-span constraint system results in a proportional increase in the stiffness of the midspan main cables, ultimately leading to an augmented overall structural stiffness. Conversely, a decrease in the stiffness of the edge-span constraint system corresponds to a reduced structural stiffness.

Second, the stiffness of the edge-span constraint system is a composite of the horizontal stiffness of the bridge tower tops and the edge-span main cables combined linearly. As the edge-to-midspan ratio increases and the bridge tower stiffness decreases, the edge-span constraint system's overall stiffness diminishes, consequently reducing the overall structural stiffness. This reduction, in turn, impacts the frequencies of the vertical bending and torsional modes of the structure, causing them to decrease.

Furthermore, due to the greater height of the Western bridge tower and the longer length of the edge span, the stiffness of the Western edge-span constraint system is

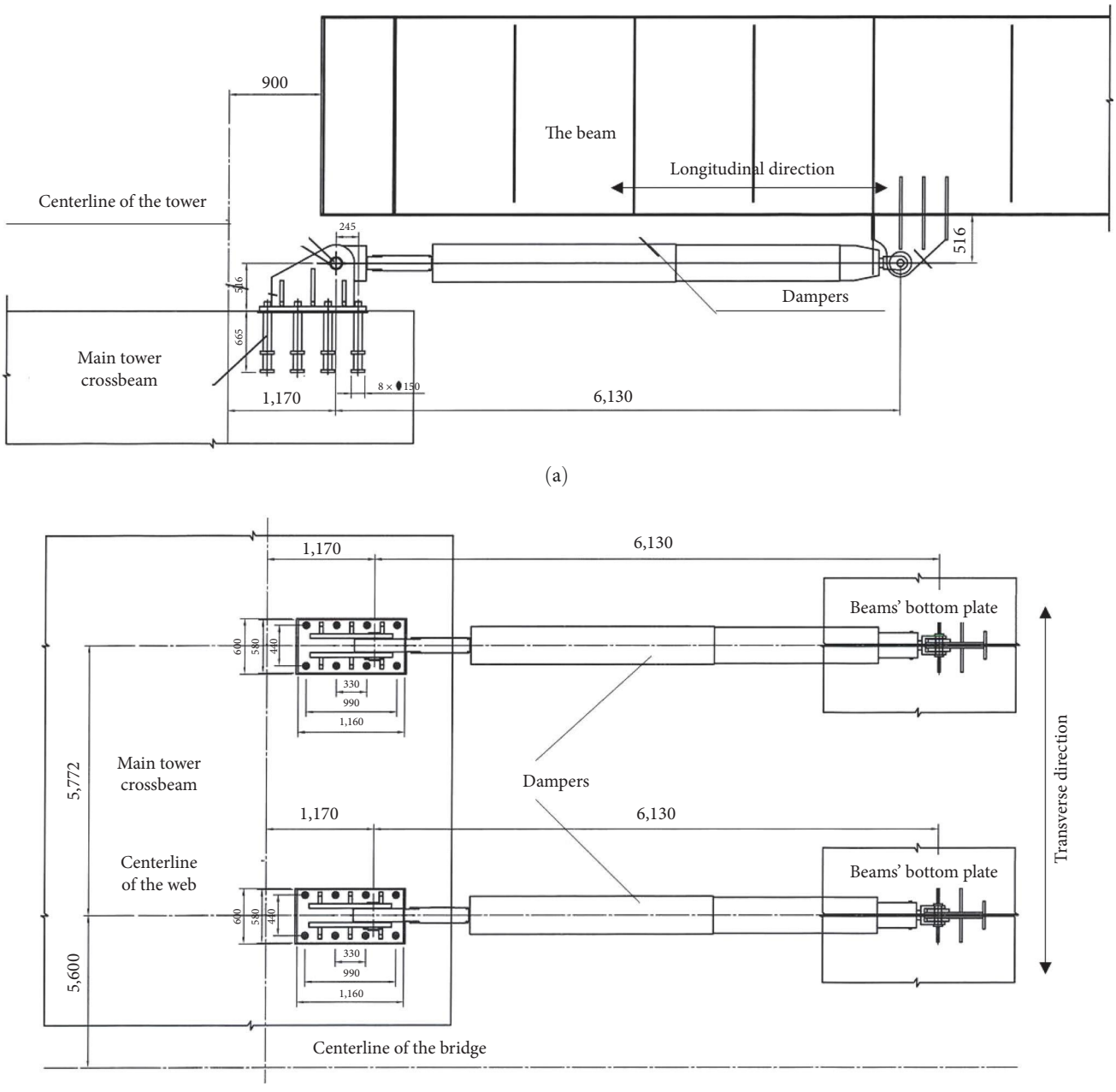

Figure 17: The arrangement of multiple groups of dampers: (a) elevation view and (b) plan layout.

comparatively lower than that of the Eastern side. Detailed calculations reveal that under live loads, the displacement at the top of the Western tower is approximately twice than that of the Eastern tower, thereby indicating that the stiffness of the Eastern edge-span constraint system is approximately twice as large as that of the Western side.

Last, by strategically adjusting the heights of the bridge towers and the edge-to-midspan ratio, it is possible to mitigate structural asymmetry and enhance the static and dynamic performance of the system. Notably, the observed asymmetry in the stiffness of the edge-span constraint system does not significantly impact the mechanical performance of the case bridge.

4.2. Parameters of the Damper. If the suspension bridge's stiffening girder adopts a structural system with no longitudinal restriction due to the extended self-vibration period, considerable displacement may happen at the end of the girder after an earthquake. Installing dampers at the connection parts of the tower and girder or at the end of the girder to increase the damping of the bridge is an effective measure to control the displacement and improve the structure's seismic performance.

The liquid viscous damper is a cylindrical pore-type damping device. The power relationship between the force and velocity of the damper is shown in Equation (12):

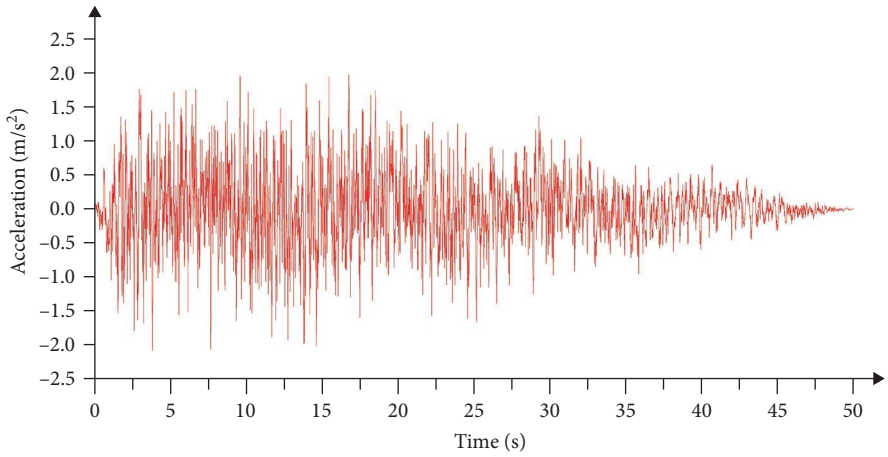

Figure 18: Seismic wave time history curve with an exceedance probability of 3% in 100 years.

$$F(t) = C\,\mathrm{sign}(\dot{u})|\dot{u}|^{\xi}, \tag{12}$$

where C is the damping coefficient, ξ is the damping exponent, and is the relative acceleration.

It can be seen from Equation (3) that at the same speed, the greater the damping coefficient C is, the greater the damping force F. Generally, the relative velocity between the tower and girder caused by seismic waves is more minor than 1 m/s, so the smaller the damping exponent ξ is, the greater the damping force F is. Although the stiffness of the damper is nonlinear, it can be seen from the above analysis that the stiffness of the damper can be increased with the rise of damping coefficient C or the decrease of damping exponent ξ.

Four groups of dampers are usually set between the towers and stiffening girders of suspension bridges, as shown in Figure 17. For convenience, the damping coefficient C in this section represents the sum of the damping coefficients of one-sided dampers. The damping exponent ξ is taken as 0.3, 0.5, 0.7, and 0.9. The damping coefficients are 2,000, 6,000, 10,000, and 14,000, respectively (the unit of damping coefficient ξ is kN/(m/s)).

Nonlinear time history analysis is used to investigate the impact of damper settings on the displacement at the end of the girder and the impact on the damping force. The artificial seismic wave generator is utilized to construct the time history curve based on the conditions at the bridge site, and four seismic waves with good fitting are chosen for input. Figure 18 depicts a seismic wave time history curve. Seismic waves have a 3% chance of exceeding their limits every 100 years.

Under the seismic circumstances, Figure 19 depicts the changing trend of the greatest relative displacement between the tower and girder with various damper values. As noticed, setting a damper efficiently reduces the relative displacement between the tower and the girder. The relative displacement falls as the damping exponent drops and decreases as the damping coefficient C increases, and the reduction speed steadily decreases.

Under the seismic circumstances, Figure 20 depicts the relationship between the maximum damping force and

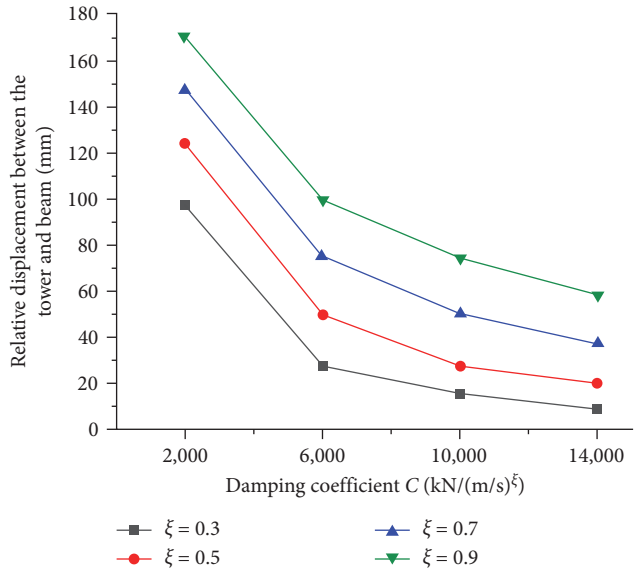

Figure 19: The maximum relative displacement between the tower and girder in the west under different damper parameters.

damper settings. It can be shown that the damping force grows as the damping exponent and damping coefficient C decrease, and the growth rate steadily declines.

Figure 21 shows the trend of the maximum moment at the tower bottom with the change of damper parameters under seismic conditions. It can be seen that the moment at the bottom of the tower increases with the reduction of damping exponent ξ and decreases with the growth of damping coefficient C, and the reduction rate decreases gradually. When ξ is taken as 0.3, the moment at the bottom of the tower increases with the rise of C.

The inclined hanger's horizontal component constrains the stiffening girder's longitudinal displacement under seismic conditions if the damper is not set. When the hanger is slanted, the imbalanced horizontal force is transmitted to the tower's top, causing a substantial moment at the tower's bottom. The longitudinal restraint reaction of the stiffening

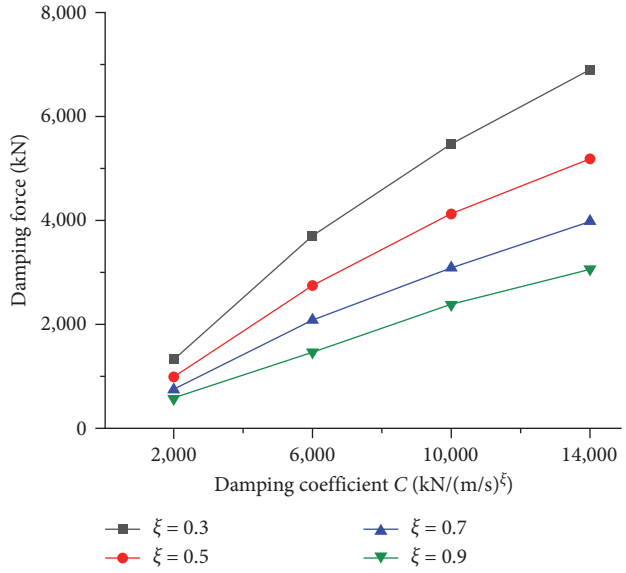

Figure 20: The maximum damping force of the west side under different damper parameters.

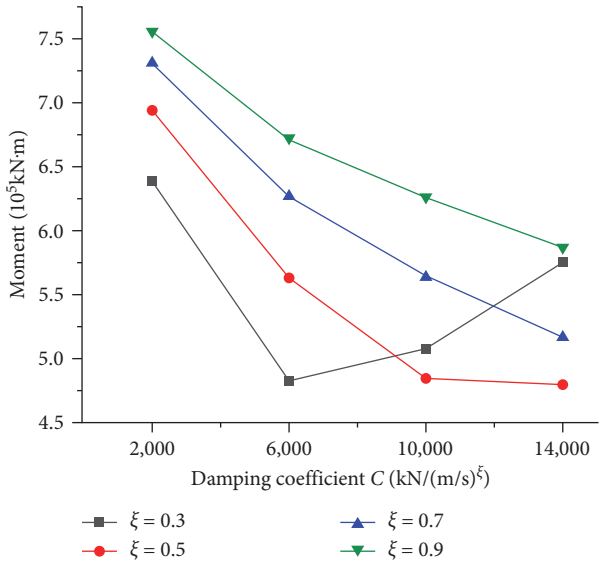

Figure 21: Maximum bottom moment of west tower under different damper parameters.

girder is conveyed to the center of the bridge tower through the damper once it is set, and the active position of the shear force in the tower goes down, resulting in a decrease in the moment at the bottom of the tower.

For different damping ratios ξ, there exists a threshold value where the bending moment at the base of the east tower remains almost unchanged with the varying damping coefficient C when C is less than this threshold. However, when C exceeds this threshold, the bending moment at the base of the east tower increases with increasing C. Moreover, this threshold value decreases as ξ decreases. This indicates that when the stiffness of the damper itself exceeds a certain threshold, the bending moment at the base of the east tower increases due to the presence of the damper, which adversely affects the force distribution on the east tower. This is attributed to the fact that the lateral stiffness of the east tower is significantly higher than that of the west tower, and when the damper stiffness is high, the east tower bears the majority of the lateral reaction forces while weakening the effectiveness of the damper on the west side.

Setting a damper can effectively minimize the displacement of the stiffening girder, as shown in Figures 19 and 21. The relative displacement between the tower and the girder reduces as C decreases. However, if C is too large or too little, the damping force will be substantial, increasing the reaction wall's design difficulties. As a result, the damper parameters should be chosen carefully to limit the relative movement of the tower and girder and to keep the damping force within a tolerable range.

5. Conclusions

Based on the characteristics of bridges in the mountainous areas, this paper proposes an improved shape-finding method for main cables, and the finite element analysis carefully studies some asymmetric parameters. The study can be summarized as follows:

(1) An improved shape-finding method considering the impact of the construction process is proposed. The hanger forces are determined by initially treating the stiffening girder as a multipoint supported continuous beam. Then, the main cable shape is calculated by an analytical method based on the equilibrium equation. A full-bridge model with the construction steps is next established in the FE software to update the hanger forces. In the iterative process, the cable shape and the hanger forces are used as input to the analytical and FE model, until the convergence of the results. The components of hanger forces in various construction steps are fully considered through the nonlinear FE model.

(2) The side-to-span ratio of the main cable and the stiffness of the tower affect the horizontal constrain stiffness of the main cable in the midspan. With a smaller side-to-span ratio or a lower tower height, the horizontal constrained stiffness of the main cable can be greater, thus resulting in reduced displacements at the tower top and along the stiffening girder under live loads. The asymmetry of the bridge layout can lead to the different horizontal displacements of the tower under live loads, which mainly affects the value of the tower's bending moments. However, it yields minor effects on the overall performance of the bridge.

(3) Setting dampers between the tower and the girder and choosing proper damper parameters can effectively minimize the longitudinal displacement of stiffening girders and benefit controlling the moment of towers under the seismic situations. Noteworthy, for towers with large differences in horizontal stiffness, excessive damping forces may considerably increase the bending moment of the higher tower.

Data Availability

Some or all data, models, or code generated or used during the study are available from the corresponding author upon reasonable request.

Conflicts of Interest

The authors declare that they have no conflicts of interest.

Acknowledgments

The authors gratefully appreciate the financial support from the National Key Research and Development Program of China (2021YFB1600300), the Scientific Research Project of China Power Construction Road and Bridge Group Co., Ltd. (HHZ-JGY-FW-07), the National Natural Science Foundation of China (51878494), and the Science and Technology Committee of Shanghai, China (21DZ1202900).

References

[1] W.-M. Zhang, C.-Y. Yang, and J.-Q. Chang, "Cable shape and construction parameters of triple-tower double-cable suspension bridge with two asymmetrical main spans," *Journal of Bridge Engineering*, vol. 26, no. 2, Article ID 04020127, 2021.

[2] N. J. Gimsing and C. T. Georgakis, *Cable Supported Bridges: Concept and Design*, John Wiley & Sons, Ltd, 2011.

[3] K.-S. Kim and H. S. Lee, "Analysis of target configurations under dead loads for cable-supported bridges," *Computers and Structures*, vol. 79, no. 29-30, pp. 2681–2692, 2001.

[4] H.-K. Kim and M.-Y. Kim, "Efficient combination of a *TCUD* method and an initial force method for determining initial shapes of cable-supported bridges," *International Journal of Steel Structures*, vol. 12, pp. 157–174, 2012.

[5] M.-Y. Kim, D.-Y. Kim, M.-R. Jung, and M. M. Attard, "Improved methods for determining the 3 dimensional initial shapes of cable-supported bridges," *International Journal of Steel Structures*, vol. 14, pp. 83–102, 2014.

[6] R. Xiao, M. Chen, and B. Sun, "Determination of the reasonable state of suspension bridges with spatial cables," *Journal of Bridge Engineering*, vol. 22, no. 9, Article ID 04017060, 2017.

[7] C. Song, R. Xiao, and B. Sun, "Improved method for shape finding of long-span suspension bridges," *International Journal of Steel Structures*, vol. 20, pp. 247–258, 2020.

[8] C. Li, J. He, Z. Zhang et al., "An improved analytical algorithm on main cable system of suspension bridge," *Applied Sciences*, vol. 8, no. 8, Article ID 1358, 2018.

[9] T. Li and Z. Liu, "A recursive algorithm for determining the profile of the spatial self-anchored suspension bridges," *KSCE Journal of Civil Engineering*, vol. 23, pp. 1283–1292, 2019.

[10] Y. Zhou and S. Chen, "Iterative nonlinear cable shape and force finding technique of suspension bridges using elastic catenary configuration," *Journal of Engineering Mechanics*, vol. 145, no. 5, 2019.

[11] W. Zhu, Y. Ge, G. Fang, and J. Cao, "A novel shape finding method for the main cable of suspension bridge using nonlinear finite element approach," *Applied Sciences*, vol. 11, no. 10, Article ID 4644, 2021.

[12] S. Wang, Z. Zhou, Y. Gao, and Y. Huang, "Analytical calculation method for the preliminary analysis of self-anchored suspension bridges," *Mathematical Problems in Engineering*, vol. 2015, Article ID 918649, 10 pages, 2015.

[13] Y. Sun, H.-P. Zhu, and D. Xu, "New method for shape finding of self-anchored suspension bridges with three-dimensionally curved cables," *Journal of Bridge Engineering*, vol. 20, no. 2, 2014.

[14] M.-Y. Kim, M.-R. Jung, and M. M. Attard, "Unstrained length-based methods determining an optimized initial shape of 3-dimensional self-anchored suspension bridges," *Computers & Structures*, vol. 217, pp. 18–35, 2019.

[15] L.-B. Wang, Y. Wu, and M. Noori, "Parameters of static response of carbon fiber reinforced polymer (CFRP) suspension cables," *Journal of Central South University*, vol. 22, pp. 3123–3132, 2015.

[16] L. Jia, Z. Lin, R. Xiao, and Y. Jiang, "Parameter effects on the mechanical performance of triple-tower four-span suspension bridges," *Advances in Structural Engineering*, vol. 21, no. 2, pp. 256–269, 2017.

[17] J. Lijun, W. Jinliang, J. Yang, and X. Rong, "A parametric study of long-span triple-tower suspension bridge," *Advances in Structural Engineering*, vol. 23, no. 15, pp. 3185–3194, 2020.

[18] J. Cheng, M. Xu, and H. Xu, "Mechanical performance analysis and parametric study of double-deck plate-truss composite steel girders of a three-tower four-span suspension bridge," *Engineering Structures*, vol. 199, Article ID 109648, 2019.

[19] H. Cao, Y. Chen, J. Li, and S. Liu, "Static characteristics analysis of three-tower suspension bridges with central buckle using a simplified model," *Engineering Structures*, vol. 245, Article ID 112916, 2021.

[20] S.-X. Zheng, X.-H. Shi, H.-Y. Jia, C.-H. Zhao, H.-L. Qu, and X.-L. Shi, "Seismic response analysis of long-span and asymmetrical suspension bridges subjected to near-fault ground motion," *Engineering Failure Analysis*, vol. 115, Article ID 104615, 2020.

[21] Z. Xu, H. Wang, H. Zhang, K. Zhao, H. Gao, and Q. Zhu, "Non-stationary turbulent wind field simulation of long-span bridges using the updated non-negative matrix factorization-based spectral representation method," *Applied Sciences*, vol. 9, no. 24, Article ID 5506, 2019.

[22] H. Tang, Y. Li, K. M. Shum, X. Xu, and Q. Tao, "Non-uniform wind characteristics in mountainous areas and effects on flutter performance of a long-span suspension bridge," *Journal of Wind Engineering and Industrial Aerodynamics*, vol. 201, Article ID 104177, 2020.

[23] J. Cheng and R.-C. Xiao, "A simplified method for lateral response analysis of suspension bridges under wind loads," *Communications in Numerical Methods in Engineering*, vol. 22, no. 8, pp. 861–874, 2006.

[24] Z. Guo, S. Lin, and Q. Ni, "Advances in active control of wind-induced vibration of long-span suspension bridges," *International Journal of Structural Stability and Dynamics*, vol. 22, no. 12, Article ID 2230002, 2022.

[25] M. Zhang, F. Jiang, J. Zhang, J. Qin, X. Jiang, and Y. Li, "Field measurement of local wind environment on the approach deck of a suspension bridge in mountain terrain," *Scientific Reports*, vol. 12, Article ID 15659, 2022.

[26] D. M. Siringoringo and Y. Fujino, "Seismic response of a suspension bridge: insights from long-term full-scale seismic monitoring system," *Structural Control and Health Monitoring*, vol. 25, no. 11, Article ID e2252, 2018.

[27] S. Arzoumanidis, A. Shama, and F. Ostadan, "Performance-based seismic analysis and design of suspension bridges," *Earthquake Engineering & Structural Dynamics*, vol. 34, no. 4-5, pp. 349–367, 2005.

[28] L. Lu, "Application of buckling-restrained braces in the seismic control of suspension bridges," *Earthquake Engineering and Engineering Vibration*, vol. 21, pp. 543–557, 2022.
[29] F. Meng, J. Wan, Y. Xia, Y. Ma, and J. Yu, "A multi-degree of freedom tuned mass damper design for vibration mitigation of a suspension bridge," *Applied Sciences*, vol. 10, no. 2, Article ID 457, 2020.